ACS APPLIED MATERIALS & INTERFACES

Research Article

www.acsami.org

Wide Range Bandgap Modulation Based on ZnO-based Alloys and Fabrication of Solar Blind UV Detectors with High Rejection Ratio

Longxing Su,[†,⊥] Yuan Zhu,*[,†,⊥] Dingyu Yong,[‡] Mingming Chen,[†] Xu Ji,[†] Yuquan Su,[†] Xuchun Gui,[†] Bicai Pan,[‡] Rong Xiang,[†] and Zikang Tang*[,†,§]

[†]State key Laboratory of Optoelectronic Materials and Technologies, School of Physics and Engineering, Sun Yat-Sen University, Guangzhou 510275, China

[‡]Department of Physics and Hefei National Laboratory for Physical Sciences at Microscale, University of Science and Technology of China, Hefei, Anhui 230026, China

[§]Physics Department, Hong Kong University of Science and Technology, Clear Water Bay, Kowloon, Hong Kong, China

ABSTRACT: Theoretical calculations on formation energies of MgZnO, BeZnO and BeMgZnO alloys are presented. The ternary alloy MgZnO (BeZnO) is found to be unstable with high Mg (Be) contents. However, the quaternary system BeMgZnO is predicted to be stable with small Be/Mg atom ratio. Subsequently, a wurtzite $Be_{0.17}Mg_{0.54}Zn_{0.29}O$ alloy with a bandgap of 5.15 eV has been acquired experimentally. Its bandgap is in the middle of solar blind region and thus it is an ideal material for realizing a high rejection ratio solar blind ultraviolet (UV) detector, which has long been a problem. A metal−semiconductor−metal (MSM) structured solar blind UV detector based on this material is then fabricated, realizing a much higher rejection ratio than reported MgZnO-based detectors. One more interesting thing is, as a complicated quaternary system, BeMgZnO can maintain its crystal quality in a wide compositional range, which is not happening in MgZnO and BeZnO. To get some microscopic insight into the Be−Mg mutual stabilizing mechanism, more calculations on the lattice constants of BeZnO and MgZnO alloys, and the coordination preference of Be ions in alloy were conducted. The *a*-axis lattice compensation and 4-fold coordination preference of Be atom are confirmed the major origins for Be−Mg mutual stabilizing in ZnO lattice.

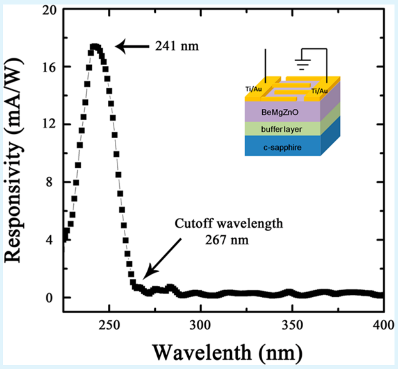

KEYWORDS: *bandgap modulation, stability, solar blind detector, high rejection ratio*

1. INTRODUCTION

ZnO is regarded as a promising wide bandgap material for the potential applications in ultraviolet region optoelectronic devices, such as light emitting diodes (LEDs), laser diodes (LDs) and ultraviolet (UV) detectors, due to its direct wide bandgap (3.37 eV) and large excition binding energy (60 meV).[1−6] Among those applications, ZnO-based solar blind photodetectors have received much attention recently for their broad applications in chemical threat detection, flame sensing, missile plume early warning and ultraviolet environmental monitoring.[7−12] The solar blind range is from the wavelength of 280 to 220 nm. Hence, bandgap modulation based on ZnO-based alloys is necessary to adjusting the bandgap of ZnO to such region. MgZnO alloy was first considered because the ion radius of Mg^{2+} (0.57 Å) is similar to that of Zn^{2+} (0.60 Å).[13] However, reproducible preparation of wurtzite MgZnO (*w*-MgZnO) with high Mg content is rather difficult due to the phase segregation of rocksalt MgZnO (*rs*-MgZnO). Ohtomo et al.[14] first observed the phased segregation of MgZnO when Mg concentration is larger than 0.33. They reported a *w*-$Mg_{0.33}Zn_{0.67}O$ alloy with a bandgap of 3.99 eV. This record was soon and barely broken by Sharma et al.,[15] who presented a *w*-$Mg_{0.36}Zn_{0.64}O$ alloy with a bandgap of 4.0 eV by using pulse laser deposition (PLD) technique. As a big step forward, Du et al.[16] employed a delicate interface control technique and achieved a *w*-$Mg_{0.55}Zn_{0.45}O$ alloy film with a bandgap of 4.55 eV (272 nm). On the basis of this *w*-$Mg_{0.55}Zn_{0.45}O$ film, they fabricated a solar blind UV detector that showed obvious responsivity. Because 272 nm is on the edge of the solar blind range, the peak broadening would surly weaken the response suppression in the solar blind range, leading to a rejection ratio (responsivity at peak/responsivity at 280 nm) as low as ∼4.7. A later work done by Zheng et al.[17] enhanced the responsivity of MgZnO solar blind UV detector; but the rejection ratio remains a problem and gets even lower to ∼1.6 as a sacrifice for the high responsivity. On the other side, BeZnO alloy as a rising alternative material attracted some research interests in recent years. In pioneering work done by Ryu et al.,[18] they demonstrated that BeZnO has a great potential in wide range bandgap engineering (3.37−10.6 eV). However, the crystallography of the same alloy category was reported in their another paper and was not as encouraging.[19] Our previous work also

Received: June 3, 2014
Accepted: August 4, 2014
Published: August 4, 2014

displayed the phase evolution and structure relaxation of BeZnO alloy and confirmed its incompetency for bandgap engineering based on both experiments and calculations.[10,20] The discouraged results can be ascribed to the large lattice mismatch between BeO ($a = 2.71$ Å, $c = 4.32$ Å) and ZnO ($a = 0.325$ Å, $c = 0.523$ Å).[18] BeMgZnO alloy was recently proposed as a balance between ZnO/MgO and ZnO/BeO.[21] However, the reported crystal quality deteriorates rapidly with the increase of Be content, which is certainly not good for device performance. This problem was nicely solved in our recent work, in which we have improved the crystal quality of this quaternary alloy to the device level and fabricated a series of UV detectors.[10] Despite this progress, the solar blind rejection ratio is still low and the Be−Mg mutual stabilizing mechanism is still unclear.

Here, we demonstrate systematic calculations on the formation energy of quaternary alloy BeMgZnO based on first principle. We also calculated the formation energies of ternary alloys as BeZnO, MgZnO and BeMgO for comparison. A series of energy saddle points suggested the potential growth windows for stable wurtzite BeMgZnO, according to which, we have experimentally acquired a quaternary alloy with a bandgap of 5.15 eV (~241 nm). On the basis of this BeMgZnO alloy, we have fabricated a metal−semiconductor−metal (MSM) structured detector. The response peak is located at 241 nm, which is in the middle of solar blind range. The response spectra are clean for wavelength larger than 280 nm and hence render a rejection ratio as high as 21. To get some microscopic insight into the Be−Mg mutual stabilization mechanism, we employed the first principle calculation again and examined the lattice constant and preferred coordination number of Be in the quaternary alloy. The *a*-axis lattice compensation caused by Be and Mg ions and 4-fold coordination preference of Be atoms are postulated to be main causes of Be−Mg mutual stabilizing in the ZnO lattice.

2. EXPERIMENTAL METHODS

2.1. Calculation Details. The first-principle density functional theory (DFT) calculations were performed using Vienna ab initio simulation packages (VASP). Generalized gradient approximation (GGA) in the Perdew−Burke−Ernzerhof (PBE)[22] form was used, and the cutoff energy was 600 eV. The structure models were constructed by using a 128-atom supercell consisting of 4 × 4 × 2 unit cells. In the first Brillouin zone, the *k*-points were sampled with 2 × 2 × 2 γ-centered Monkhorst−Pack meshes.[23] Based on the *k*-point convergence tests, finer meshes resulted in total-energy changes of <1 meV/atom. By computing the quantum mechanical forces and stress tensor, the special quasirandom structures (SQSs)[24] were fully relaxed with respect to both the volume and shape of the unit cell, as well as all the internal atomic positions using the conjugation gradient algorithm. And the energy minimization was converged until the force on each atom is less than 0.02 eV/Å. The formation energy of ternary alloy was calculated by using the following equation:[25]

$$\Delta E_f(x, y) = E(A_xB_yC_{1-x-y}D) - xE(AD) - yE(BD) - (1 - x - y)CD$$

Where x, y is the Be, Mg concentration, $E(A_xB_yC_{1-x-y}D)$, $E(AD)$, $E(BD)$ and $E(CD)$ is the total energy of the corresponding systems $Be_xMg_yZn_{1-x-y}O$, BeO, MgO and ZnO, respectively.

2.2. Sample Preparation and Measurement. The $Mg_xZn_{1-x}O$, $Be_xZn_{1-x}O$ and $Be_xMg_yZn_{1-x-y}O$ alloy films were grown on *c*-plane sapphire by means of radio-frequency plasma-assisted molecular beam epitaxy (rf-MBE) technique. Elemental Be (4N), Zn (6N), and Mg (6N) were evaporated using Knudsen cells. Active oxygen radicals were generated by an rf-plasma system (SVTA) using high purity oxygen gas (6N). Before growth, the sapphire substrate was ultrasonically cleaned in acetone and followed in ethanol for 15 min, respectively. Then the substrate was rinsed in deionized water and dried with a nitrogen gun. After that, it was thermally cleaned at 750 °C in a vacuum for 20 min. For the growth of $Mg_xZn_{1-x}O$ ($Be_xZn_{1-x}O$), the content of Mg (Be) is adjusted by varying the Mg (Be) source temperature while other conditions are set. For the growth of $Be_xMg_yZn_{1-x-y}O$, the Mg and Be source temperature vary at the same time with other condition set. The lattice structure and crystal quality of the alloy crystal films were studied by X-ray diffraction (XRD, Rigaku, D-MAX 2200 VPC). High-resolution transmission electron microscopy (HRTEM, JEM 100CXII, JEOL) was used to clarify the crystal structure of the alloy film. The element composition of each alloy was determined by the X-ray photoelectron spectroscopy (XPS, ESCALAB 250). The absorption spectra were measured using ultraviolet−visible-near-infrared (UV−vis-NIR) scanning spectrometry (Shimadzu, UV-3150).

2.3. Device Fabrication and Measurement. The MSM structure photodetector was fabricated by depositing Ni/Au interdigital finger layers onto the alloy film. The interdigital structure was fabricated via a standard photolithography and electron beam evaporation technique. The length, width and spacing of the interdigital fingers are 2 mm, 20 and 15 μm, respectively. The optical response of the photodetector was recorded by a semiconductor parameter analyzer (Keithely 2200), using 150 W Xe lamp as the light source. The measurement was taken under the condition of 40 V bias.

3. RESULTS AND DISCUSSION

First, $Mg_xZn_{1-x}O$ and $Be_xZn_{1-x}O$ alloys were investigated for understanding the structural properties and phase segregation micromechanism of corresponding ternary alloy systems. Figure 1a shows the formation energies ($\Delta E_f(x)$) of wurtzite- and rocksalt-phase $Mg_xZn_{1-x}O$ alloys with different Mg concentrations. In ternary alloy system, larger $\Delta E_f(x)$ suggests a less stable system in comparison with the binary compound (ZnO, MgO) and vise versa. Obviously, the formation energies of wurtzite-phase $Mg_xZn_{1-x}O$ alloys increase linearly as Mg contents and the rocksalt-phase $Mg_xZn_{1-x}O$ alloys reveal the opposite variation tendency. By comparing the calculated $\Delta E_f(x)$, we can make a conclusion that low Mg concentration $Mg_xZn_{1-x}O$ alloys will be more order and stable in wurtzite-phase structure and high Mg concentration $Mg_xZn_{1-x}O$ alloys will be more order and stable in rocksalt-phase structure. Interestingly, the phase transition point of wurtzite-phase to rocksalt-phase was found at $x = 0.33$ (indicated by the blue arrow in Figure 1a), which is consistent well with experimental findings.[14] Figure 1b reveals the formation energies of $Be_xZn_{1-x}O$ alloys with different Be contents. Low- and high-Be content $Be_xZn_{1-x}O$ alloys were relatively stable due to their small formation energies. However, $Be_xZn_{1-x}O$ alloys with intermediate Be content were quite unstable and easily segregated into low- and high-Be content phases due to their large formation energies. The calculated results were quite reasonable for $Be_xZn_{1-x}O$ alloys because the large lattice mismatch between BeO and ZnO.

The theoretical predictions of ternary alloy $Mg_xZn_{1-x}O$ and $Be_xZn_{1-x}O$ were then confirmed by our experimental results. Figure 2a exhibits the SEM (HITACHI, S-4800) image of $Mg_{0.33}Zn_{0.67}O$. Rectangular shaped precipitates of about 150 × 40 nm size were shown by the arrows, which indicate the initiation of phase segregation. The SEM image of $Be_{0.42}Zn_{0.58}O$ in Figure 2b shows a typical multicrystal morphology with particle size of around tens to hundreds of nanometers. The hexagonal feature is less indistinct, owing to the large lattice

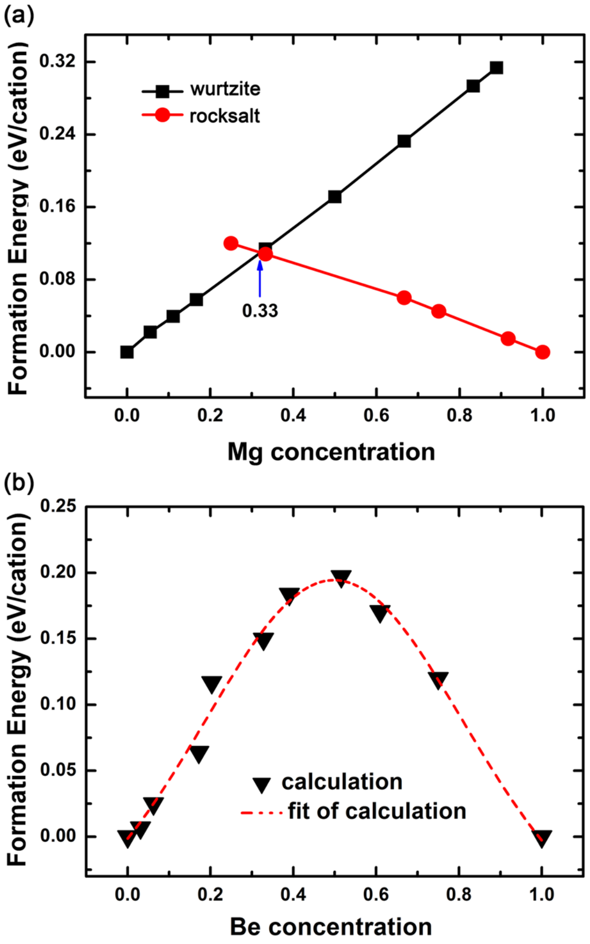

Figure 1. (a) Formation energies of wurtzite and rocksalt $Mg_xZn_{1-x}O$ as a linear function of Mg concentrations, the phase transition point is found to be 0.33; (b) formation energies of $Be_xZn_{1-x}O$ as a function of Be concentrations, $Be_xZn_{1-x}O$ with intermediate Be content has the highest formation energy.

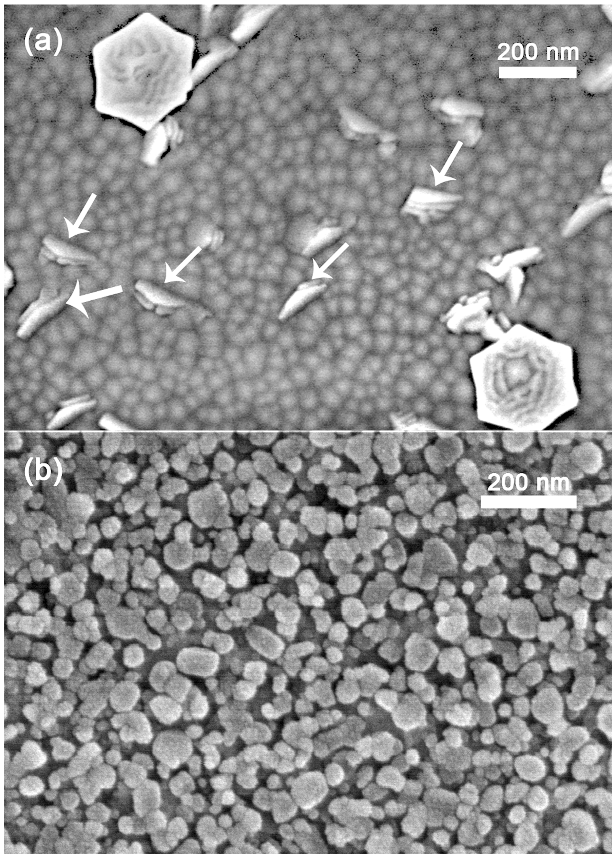

Figure 2. (a) SEM image of $Mg_{0.33}Zn_{0.67}O$. The cubic precipitates of $Mg_{0.33}Zn_{0.67}O$ are obvious as can be seen from the grains with right angle, indicating a wutzite-to-rocksalt phase change has already happened; (b) SEM image of $Be_{0.42}Zn_{0.58}O$. A typical multicrystal morphology with particle size around tens to hundreds nanometers is shown. The hexagonal feature is indistinct owing to the poor crystal quality.

distortion in $Be_{0.42}Zn_{0.58}O$. The phase segregation of $Be_{0.42}Zn_{0.58}O$ was also verified by XRD measurement (not shown here).

According to the research above, due to the inevitable phase segregation, both $Mg_xZn_{1-x}O$ and $Be_xZn_{1-x}O$ encounter serious bottleneck in modulating the bandgap to solar blind range. Hence, we turn to quaternary alloy $Be_xMg_yZn_{1-x-y}O$, in which the lattice mismatch between ZnO/MgO and BeO/ZnO will be counteracted by each other.[26] Before fabricating a quaternary alloy $Be_xMg_yZn_{1-x-y}O$, exploring the structural characteristics of another ternary alloy $Be_xMg_{1-x}O$ is necessary for understanding the stable micromechanism of $Be_xMg_yZn_{1-x-y}O$. The calculated formation energies of $Be_xMg_{1-x}O$ alloys below suggest that the solid solubility of hexagonal MgO in the BeO host is much higher than that in the ZnO host. The upper limit (transition point) of the solid solubility was determined by the compositional wurtzite-rocksalt phase transition point of the $Be_xMg_{1-x}O$ alloys. The formation energies of rocksalt $Be_xMg_{1-x}O$ and wurtzite $Be_xMg_{1-x}O$ are presented in Figure 3a as a function of Mg content. The intersection of the two fitted curve is around 83%. For Mg content smaller than 83%, the system can readily maintain a wurtzite structure with a lower energy. For Mg content larger than 83%, the wurtzite-rocksalt phase transition would occur because the rocksalt phase then has a lower energy. This critical value 83% is much higher than the value of 33% as calculated in MgZnO system. Similar methods were used to retrieve the phase transition points for $Be_xMg_yZn_{1-x-y}O$ alloys. Figure 3b displays the resultant phase transition points in which the Be and Mg contents were given, and the Zn content can be calculated accordingly. The Be content and Mg content are basically in a linear relation and are thus linear fitted. The dotted fitting line can be taken as a phase transition line, which divides the region into two zones. Above the line is the rocksalt zone and below is the wurtzite zone. The transition points clearly show that BeO can enhance the solubility of hexagonal MgO in ZnO, only the Be/Mg atom ratio should be kept at a low level. Additionally, the more the Zn content, the lower the Be/Mg ratio. Nevertheless, the phase transition points are not the necessary optimum growth windows because they are derived from the comparison between the formation energies of rocksalt and wurtzite structures. For such a complicated quaternary system, the absolute values of energy for both structures may still be high and lead to a poor crystal quality. Thus, we turned to search the energy saddle points within the wurtzite zone for BeMgZnO alloys and Figure 3c exhibits some results. For pure BeZnO ($y = 0$), the formation energies increase monotonically with the increase of Be content. This is nonnegotiable due to the large lattice mismatch between BeO and ZnO. But for BeMgZnO alloys, the energy saddle points do exist. When $x + y = 0.33$, the saddle point is located at $x =$

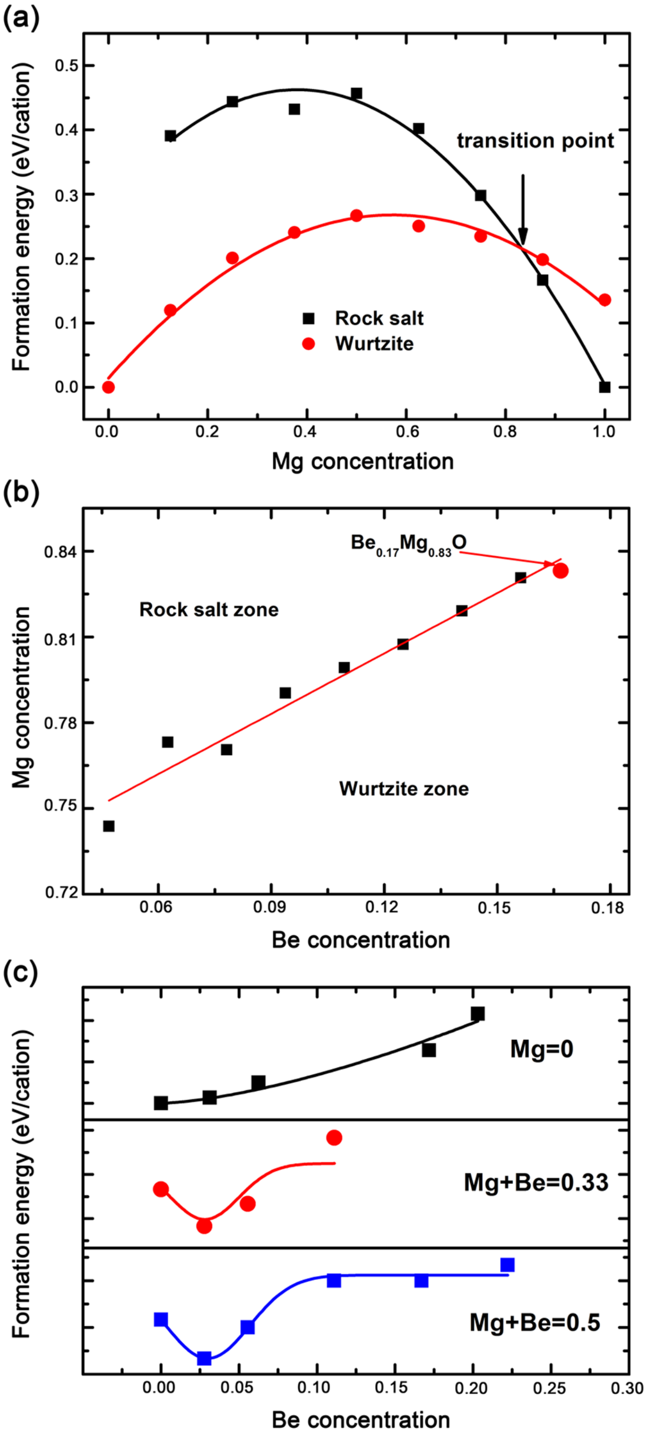

Figure 3. (a) Calculated formation energy of $Be_xMg_{1-x}O$ as a function of Mg concentration. Two possible structures are studied. Red circles denote the wurtzite structures and black squares denote the rock-salt structures. The intersection of the two curves is the wurtzite-to-rocksalt phase transition point. For $x < 0.83$, the wurtzite alloys are lower in energy than their rock-salt counterparts and hence more stable. (b) Calculated wurtzite-to-rocksalt phase transition points of $Be_xMg_yZn_{1-x-y}O$ system as a function of Be concentration. The phase transition point of MgBeO alloy derived from panel a is provided as a reference, indicated with a red circle. (c) Calculated formation energy of wurtzite $Be_xMg_yZn_{1-x-y}O$ alloy as a function of Be concentration. Three settings are considered: $y = 0$ for pure BeZnO, $x + y = 0.33$ and $x + y = 0.5$. The ternary alloy has no energy saddle point whereas each quaternary alloy has one saddle point, suggesting a growth window.

0.027. When $x + y = 0.50$, the saddle point is located at $x = 0.034$. Both suggest that the Be/Mg ratio should be kept lower than 1/10. With the knowledge of these Be/Mg ratios, we have grown a series of quaternary alloys with the MBE technique. It was soon noticed that there is a discrepancy between the calculation and the experiment. With Be content as low as 0.02, we acquired a $Be_{0.02}Mg_{0.57}Zn_{0.41}O$ alloy as reported elsewhere.[9] Although responding in the solar blind range, the steepness of the cutoff edge (Figure 2 in reference 9) is relatively poor compared with pure ZnO or MgZnO. This could be a sign for the less satisfactory crystal quality, which may account for our numerous failures in the later attempts on devices. Therefore, we increase the Be content to the range of 0.05−0.2 and the resultant alloys are displayed in Figure 4. The XRD patterns (Figure 4a) show two peaks for each sample. One is corresponding to the sapphire substrate and the other to the alloy film. The alloy peak close to the ZnO (002) is confirmed as the *w*-BeMgZnO (002) with HRTEM imaging of $Be_{0.17}Mg_{0.54}Zn_{0.29}O$, as shown in Figure 5. With increasing

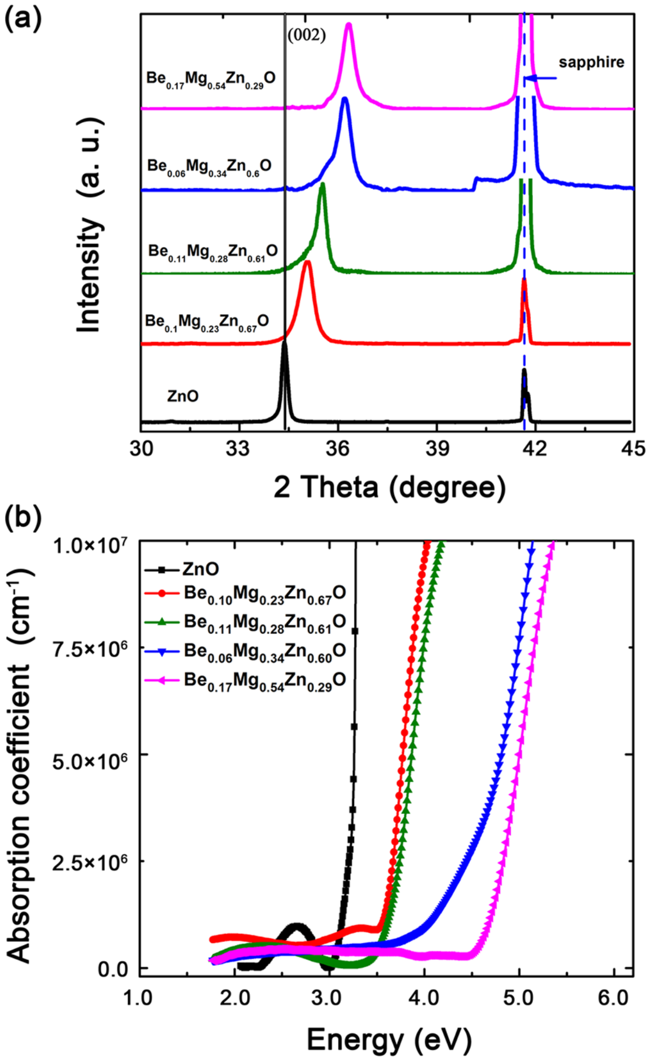

Figure 4. (a) XRD patterns of quaternary alloy $Be_xMg_yZn_{1-x-y}O$ samples. No phase segregation is observed and the crystal quality maintains well in a doping range as wide as 0.33 to 0.71. (b) Absorption spectra of corresponding $Be_xMg_yZn_{1-x-y}O$ alloys. $Be_{0.17}Mg_{0.54}Zn_{0.29}O$ illustrates a widest band gap of 5.15 eV, which is in the middle of the solar blind region.

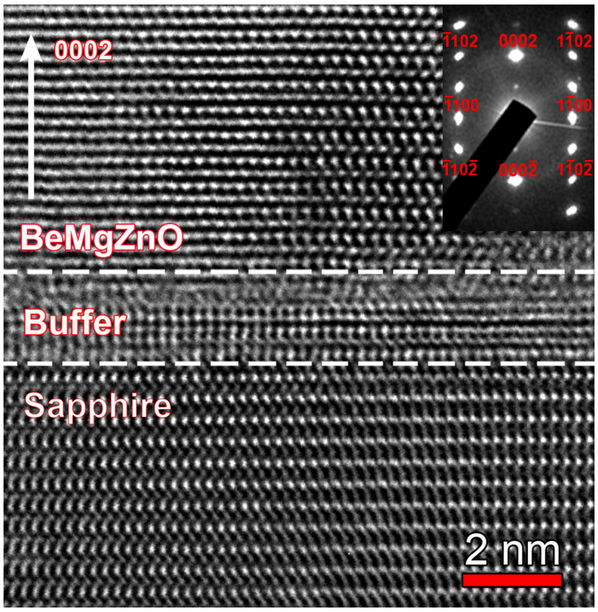

Figure 5. Cross-sectional HRTEM image of $Be_{0.17}Mg_{0.54}Zn_{0.29}O/BeO/Al_2O_3$ layered structure along (0002). Inset is the selected area electron diffraction of $Be_{0.17}Mg_{0.54}Zn_{0.29}O$.

doping level, the *w*-BeMgZnO (002) peak moves continuously toward large angle side yet with a constant FWHM (full width at half-maximum). The latter phenomenon is very unusual within a doping range as wide as 0.33−0.71. It is quite unlike the crystal quality deterioration occurred in BeZnO system,[19,20] or the rocksalt phase segregation that occurred in the MgZnO system.[14] On one side, this indicates the success of keeping a relatively low Be/Mg ratio similar to calculated results. On the other side, this exception is a strong hint for the existence of a special Be−Mg mutual stabilizing mechanism that we will discuss later.

Figure 4b presents the absorption spectra of the quaternary alloys. It is noticeable that the bandgap of $Be_{0.17}Mg_{0.54}Zn_{0.29}O$ is as high as 5.15 eV (241 nm), which is in the middle of the solar blind region and 0.6 eV higher than the best reported for MgZnO (4.55 eV).[8,16] Among these quaternary alloys, the $Be_{0.06}Mg_{0.34}Zn_{0.60}O$ was also paid attention to due to its lowest Be/Mg ratio (0.176). This value is closest to the predicted one, yet it turns out doing no good to the steepness of the cutoff edge, as shown in the absorption spectra (Figure 4b). Unlike the other three, its lower energy side of the cutoff slope is very tilting. Although its cutoff edge can be counted as in the solar blind range, this tilting will yet result in a poor rejection ratio. But this is not likely to be the case for the other three alloys with better steepness. Their Be/Mg ratios are around 0.3−0.4. As predicted in Figure 3b, it is not the Be content or Mg content that matters; it is the Be/Mg ratio that matters. Although the practical Be/Mg ratios are not exactly as the predicted ones, they share the same rule: keeping Be/Mg atom ratio low. Moreover, this discrepancy between experiments and calculations can be attributed to the growth technique we used. MBE itself is a very nonequilibrium method, which cannot fully reflect the equilibrium circumstance as set in the calculations.

On the basis of the three BeMgZnO alloys with better steepness, MSM-structured UV detectors were fabricated. The detectors on $Be_{0.1}Mg_{0.23}Zn_{0.67}O$ and $Be_{0.11}Mg_{0.28}Zn_{0.61}O$ were reported elsewhere,[10] whereas the solar blind one on $Be_{0.17}Mg_{0.54}Zn_{0.29}O$ is demonstrated in Figure 6. Figure 6a shows the current−voltage (*I*−*V*) characteristic of $Be_{0.17}Mg_{0.54}Zn_{0.29}O$ based MSM detector in the dark and 241 nm illumination. The *I*−*V* curve indicates a clearly Schottky contact behavior of the MSM detector. Under 5 V bias, the dark current was as low as 9.3 pA, which indicated the high material resistivity and Schottky barrier height. Figure 6b presents the responsivity as a function of the wavelength for the solar blind detector, inset is the schematic diagram of the MSM detector. The peak response is found at 241 nm (~18 mA/W), which is in the middle of the solar blind range. The response drops to near 0 at ~270 nm and for the wavelength larger than 280 nm in the solar range, there is almost no response. The rejection ratio (peak/280 nm) is then determined as high as 21, much higher than the best reported for MgZnO,[16,17] which indicates that the device can work well in the UV region in an environment of solar radiation, while greatly suppress any response to the sunlight. We also measured the photoresponse current after 10 months and revealed that detector is very stable.

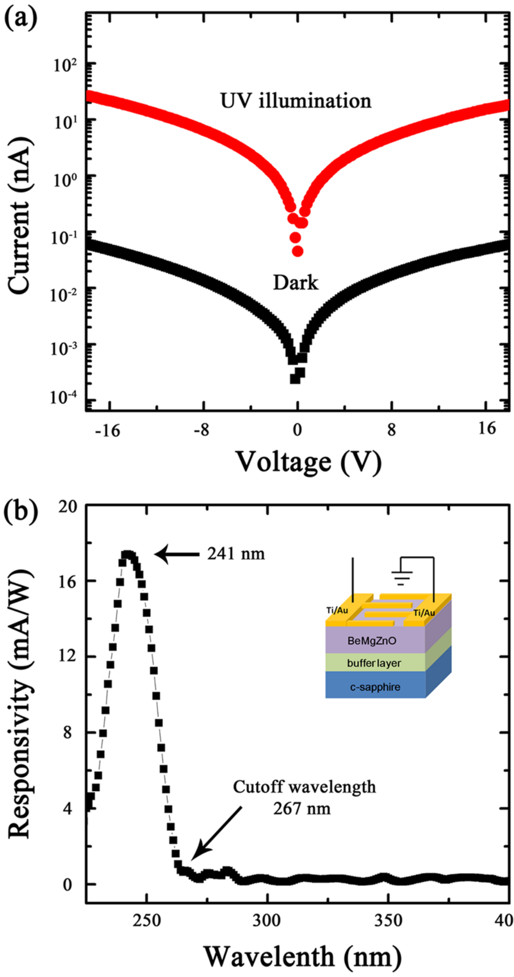

Figure 6. (a) I−V characteristic of the $Be_{0.17}Mg_{0.54}Zn_{0.29}O$ solar blind photodetector in dark and 241 nm illumination. The inset shows a schematic diagram of MSM structure solar blind UV detector. (b) Response spectra of the detector at 40 V bias, demonstrating a sharp cutoff wavelength at 267 nm.

To better understand the mutual stabilizing mechanism for Be and Mg in ZnO host from the microscopic aspect, more calculations on structure information were carried out. We first considered the *c*-parameter of the MgZnO and BeZnO, both *c*-

axis parameters of MgZnO and BeZnO decrease with increasing Mg and Be content. However, the situation of *a*-axis parameter is quite different. Figure 7a shows the calculated *a*-axis lattice parameter of BeZnO (MgZnO) as a function of Be (Mg) concentrations. The value of MgZnO increases slightly as Mg content increases, whereas BeZnO exhibits an opposite trend. As a result, in the BeMgZnO system, Be substitution induces tensile strain in the *a*-direction and somewhat compensates the compressive strain caused by Mg substitution. Because the variation in *a*-axis parameter for BeZnO is larger than that for MgZnO, the Be/Mg content ratio should be kept at a low level. Figure 7b,c exhibits the Be atoms in wurtzite (CN4) and rocksalt (CN6) $Be_xMg_{1-x}O$ alloy. In the CN4 lattice, Be atom forms strong chemical bonds with four first neighboring O atoms. And these Be−O bonds are very stable because of the strong PDOS (projective density of state) hybridization between Be and O orbits. However, in the CN6 lattice, Be−O bonds only formed between Be atoms and their three neighboring O atoms. This asymmetric bonding environment leads to the collapse of the 6-fold-coordination. Be atoms actually occupy a corner of the O octahedral interstitials rather than the center of them. This may be owing to the small radius of Be atoms, because Mg atoms are always stuck in the center of the interstitial; regardless, it is CN4 or CN6 (not shown here). This CN4 preference of Be atom should enhance the lattice distortion and system energy in the CN6 structure and make it unstable. The same results are also found in BeMgZnO systems. Thus, appropriate Be doping can effectively prevent the BeMgZnO alloy from the wurtzite-to-rocksalt phase transition.

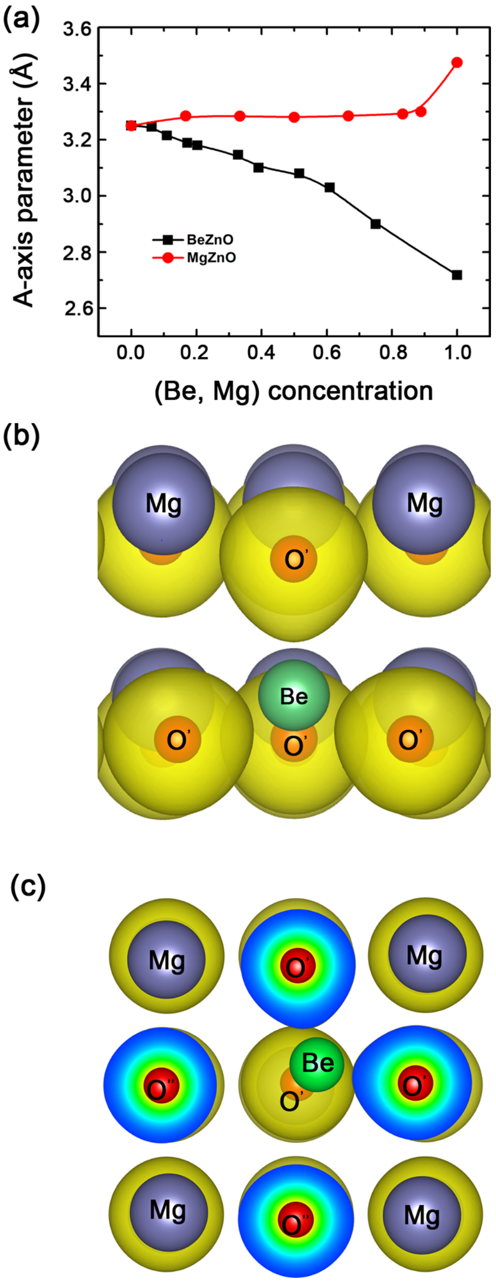

Figure 7. (a) Calculated *a*-axis parameters of $Mg_xZn_{1-x}O$ ($Be_xZn_{1-x}O$) as a function of Mg (Be) concentration. Two alloys exhibit opposite trends. (b) Calculated microstructure and charge density of wurtzite $Be_xMg_{1-x}O$ system. It is clear that Be atom is bonded to four nearest neighbor O atoms (indicated as O') and locates at the center of the tetrahedral interstitial. (c) Calculated microstructure and charge density of rock-salt $Be_xMg_{1-x}O$ system. Be atom is located off-center in the octahedral interstitial and only bonded to three neighbor O atoms (indicate as O'). O" represents the other three O atoms that are not bonded to Be atom and one of them is not shown in the figure due to the projection. Here, the balls with different color represent the charge density of different atoms.

4. CONCLUSIONS

In summary, we have systematically studied the formation energy of BeZnO, MgZnO, BeMgO and BeMgZnO alloys using first principle calculations. A useful guidance for experimental growth of stable BeMgZnO was proposed and verified. The key magic is to keep the Be/Mg ratio moderately low as 0.3−0.4. Within this, we acquired a *w*-$Be_{0.17}Mg_{0.54}Zn_{0.29}O$ alloy with bandgap of 5.15 eV, which is 0.6 eV higher than the best reported for solar blind MgZnO (4.55 eV) and is in the middle of solar blind range. On the basis of this material, we have fabricated an MSM-structured solar blind UV detector, realizing a high rejection ratio (response at peak/response at 280 nm) of 21. Moreover, with the above-mentioned magic Be/Mg ratio, we are able to tune the doping level and engineer the bandgap in a wide range, while keeping the high crystal quality. This is unusual and has never occurred to BeZnO and MgZnO systems. Thus, there must be a special mutual stabilization between Be and Mg in the ZnO host. To get some microscopic insight into its mechanism, more calculations on the lattice constants of BeZnO and MgZnO alloys, and the coordination preference of Be and Mg ions were conducted. The *a*-axis lattice compensation and 4-fold coordination preference of Be atom has been confirmed the major origins for Be−Mg mutual stabilizing in the hexagonal lattice. Our findings provide a new pathway to high quality solar blind UV detectors based on the novel quaternary alloy BeMgZnO. The resultant bandgap and rejection ratio in the solar blind region are among or may be the best ever recorded.

■ AUTHOR INFORMATION

Corresponding Authors

*Y. Zhu. E-mail: zhuy9@mail.sysu.edu.cn.
*Z. Tang. E-mail: phzktang@ust.hk.

Author Contributions

⊥L.S. and Y.Z. contributed equally to this work.

Notes

The authors declare no competing financial interest.

■ ACKNOWLEDGMENTS

This work was supported by National Key Basic Research Program of China (No. 2011CB302000), National Natural Science Foundation of China (No. 51232009 and No. 51202299) and the Fundamental Research Funds for the Central Universities (No. 11lgpy16).

■ REFERENCES

(1) Tang, Z.; Wong, G. K.; Yu, P.; Kawasaki, M.; Ohtomo, A.; Koinuma, H.; Segawa, Y. Room-Temperature Ultraviolet Laser Emission from Self-Assembled ZnO Microcrystallite Thin Films. *Appl. Phys. Lett.* **1998**, *72*, 3270−3272.

(2) Zu, P.; Tang, Z.; Wong, G. K.; Kawasaki, M.; Ohtomo, A.; Koinuma, H.; Segawa, Y. Ultraviolet Spontaneous And Stimulated Emissions from ZnO Microcrystallite Thin Films At Room Temperature. *Solid State Commun.* **1997**, *103*, 459−463.

(3) Tsukazaki, A.; Ohtomo, A.; Onuma, T.; Ohtani, M.; Makino, T.; Sumiya, M.; Ohtani, K.; Chichibu, S. F.; Fuke, S.; Segawa, Y. Repeated Temperature Modulation Epitaxy for p-Type Doping And Light-Emitting Diode Based On ZnO. *Nat. Mater.* **2005**, *4*, 42−46.

(4) Look, D. C. Recent Advances in ZnO Materials and Devices. *Mater. Sci. Eng., B* **2001**, *80*, 383−387.

(5) Kim, J. H.; Kim, E. M.; Andeen, D.; Thomson, D.; DenBaars, S. P.; Lange, F. F. Growth of Heteroepitaxial ZnO Thin Films on GaN-Buffered Al_2O_3 (0001) Substrates by Low-Temperature Hydrothermal Synthesis at 90 °C. *Adv. Funct. Mater.* **2007**, *17*, 463−471.

(6) Lupan, O.; Pauporté, T.; Le Bahers, T.; Viana, B.; Ciofini, I. Wavelength-Emission Tuning of ZnO Nanowire-based Light-Emitting Diodes by Cu Doping: Experimental and Computational Insights. *Adv. Funct. Mater.* **2011**, *21*, 3564−3572.

(7) Collins, C.; Chowdhury, U.; Wong, M.; Yang, B.; Beck, A.; Dupuis, R.; Campbell, J. Improved Solar-Blind Detectivity Using an $Al_xGa_{1-x}N$ Heterojunction p−i−n Photodiode. *Appl. Phys. Lett.* **2002**, *80*, 3754−3756.

(8) Hou, Y.; Mei, Z.; Liu, Z.; Zhang, T.; Du, X. $Mg_{0.55}Zn_{0.45}O$ Solar-Blind Ultraviolet Detector With High Photoresponse Performance and Large Internal Gain. *Appl. Phys. Lett.* **2011**, *98*, 103506.

(9) Su, L.; Zhu, Y.; Zhang, Q.; Chen, M.; Ji, X.; Wu, T.; Gui, X.; Pan, B.; Xiang, R.; Tang, Z. Solar-Blind Wurtzite MgZnO Alloy Films Stabilized by Be Doping. *J. Phys. D: Appl. Phys.* **2013**, *46*, 245103.

(10) Su, L.; Zhu, Y.; Zhang, Q.; Chen, M.; Wu, T.; Gui, X.; Pan, B.; Xiang, R.; Tang, Z. Structure and Optical Properties of Ternary Alloy BeZnO and Quaternary Alloy BeMgZnO Films Growth by Molecular Beam Epitaxy. *Appl. Surf. Sci.* **2013**, *274*, 341−344.

(11) Xie, X.; Zhang, Z.; Li, B.; Wang, S.; Jiang, M.; Shan, C.; Zhao, D.; Chen, H.; Shen, D. Mott-Type $Mg_xZn_{1-x}O$-based Visible-Blind Ultraviolet Photodetectors with Active Anti-Reflection Layer. *Appl. Phys. Lett.* **2013**, *102*, 231122.

(12) Hou, Y.; Mei, Z.; Liang, H.; Ye, D.; Liang, S.; Gu, C.; Du, X. Comparative Study of n-MgZnO/p-Si Ultraviolet-B Photodetector Performance with Different Device Structures. *Appl. Phys. Lett.* **2011**, *98*, 263501.

(13) Ghosh, R.; Basak, D. Composition Dependent Ultraviolet Photoresponse in $Mg_xZn_{1-x}O$ Thin Films. *J. Appl. Phys.* **2007**, *101*, 113111.

(14) Ohtomo, A.; Kawasaki, M.; Koida, T.; Masubuchi, K.; Koinuma, H.; Sakurai, Y.; Yoshida, Y.; Yasuda, Y.; Segawa, Y. $Mg_xZn_{1-x}O$ as a II−VI Widegap Semiconductor Alloy. *Appl. Phys. Lett.* **1998**, *72*, 2466−2468.

(15) Sharma, A.; Narayan, J.; Muth, J.; Teng, C.; Jin, C.; Kvit, A.; Kolbas, R.; Holland, O. Optical and Structural Properties of Epitaxial $Mg_xZn_{1-x}O$ Alloys. *Appl. Phys. Lett.* **1999**, *75*, 3327−3329.

(16) Du, X.; Mei, Z.; Liu, Z.; Guo, Y.; Zhang, T.; Hou, Y.; Zhang, Z.; Xue, Q.; Kuznetsov, A. Y. Controlled Growth of High-Quality ZnO-based Films and Fabrication of Visible-Blind and Solar-Blind Ultra-Violet Detectors. *Adv. Mater.* **2009**, *21*, 4625−4630.

(17) Zheng, Q.; Huang, F.; Ding, K.; Huang, J.; Chen, D.; Zhan, Z.; Lin, Z. MgZnO-based Metal-Semiconductor-Metal Solar-Blind Photodetectors on ZnO Substrates. *Appl. Phys. Lett.* **2011**, *98*, 221112.

(18) Ryu, Y.; Lee, T.; Lubguban, J.; Corman, A.; White, H.; Leem, J.; Han, M.; Park, Y.; Youn, C.; Kim, W. Wide-Band Gap Oxide Alloy: BeZnO. *Appl. Phys. Lett.* **2006**, *88*, 052103.

(19) Kim, W.; Leem, J.; Han, M.; Park, I. W.; Ryu, Y.; Lee, T. Crystalline Properties of Wide Band Gap BeZnO Films. *J. Appl. Phys.* **2006**, *99*, 096104.

(20) Chen, M.; Zhu, Y.; Su, L.; Zhang, Q.; Chen, A.; Ji, X.; Xiang, R.; Gui, X.; Wu, T.; Pan, B. Formation Behavior of $Be_xZn_{1-x}O$ Alloys Grown by Plasma-Assisted Molecular Beam Epitaxy. *Appl. Phys. Lett.* **2013**, *102*, 202103.

(21) Yang, C.; Li, X.; Gu, Y.; Yu, W.; Gao, X.; Zhang, Y. ZnO based Oxide System with Continuous Bandgap Modulation from 3.7 to 4.9 eV. *Appl. Phys. Lett.* **2008**, *93*, 112114.

(22) Perdew, J. P.; Burke, K.; Ernzerhof, M. Generalized Gradient Approximation Made Simple. *Phys. Rev. Lett.* **1996**, *77*, 3865.

(23) Monkhorst, H. J.; Pack, J. D. Special Points for Brillouin-Zone Integrations. *Phys. Rev. B* **1976**, *13*, 5188−5192.

(24) Wei, S.; Ferreira, L.; Bernard, L.; Zunger, A. Electronic Properties of Random Alloys: Special Quasirandom. *Phys. Rev. B* **1990**, *42*, 9622.

(25) Fan, X.; Zhu, Z.; Ong, Y. S.; Lu, Y.; Shen, Z.; Kuo, J. L. A Direct First Principles Study on the Structure and Electronic Properties of $Be_xZn_{1-x}O$. *Appl. Phys. Lett.* **2007**, *91*, 121121.

(26) Su, X.; Si, P.; Hou, Q.; Kong, X.; Cheng, W. First-Principles Study on The Bandgap Modulation of Be and Mg Co-Doped ZnO Systems. *Phys. B* **2009**, *404*, 1794−1798.